Evidence for truncated octahedral structures in supported gold clusters

A. Pinto, A. R. Pennisi, and G. Faraci
Dipartimento di Fisica, Università di Catania and Istituto Nazionale di Fisica della Materia, corso Italia 57, 95129 Catania, Italy

G. D'Agostino
Ente per le Nuove Technologie, l' Energia e l' Ambiente, Centro Ricerche Energetiche, Casaccia, 00100 Roma, Italy

S. Mobilio
Dipartimento di Energetica, Università dell' Aquila, Roio Monteluco, 67100 L'Aquila, Italy

F. Boscherini
Istituto Nazionale di Fisica Nucleare, 00044 Frascati, Italy
(Received 5 July 1994; revised manuscript received 21 October 1994)

Gold clusters deposited by evaporation on a Mylar substrate in many superimposed layers have been studied by EXAFS (extended x-ray-absorption fine-structure) spectroscopy at $T=28$ K. For such clusters, the first shell signal of the EXAFS spectrum has been compared with the corresponding crystal data used for the phase and amplitude calibration. The simulation of the EXAFS spectra for different possible geometrical structures (cubo-octahedral, icosahedral, truncated octahedral) applying a curved wave method with a set of theoretically calculated parameters (nearest-neighbor distance, coordination, and Debye-Waller factor) provided reference curves for the experimental data. A complete analysis including the cumulants of the radial distribution, the dispersion of the cluster sizes given by electron microscopy, and a decomposition in partial contributions obtained by a minimization method, allowed us to determine that the dominant geometrical structure of the clusters is truncated octahedral. In contrast with recent theoretical calculations, we show that the interatomic distance of gold nanoparticles results indeed contracted, independently of the use of the cumulants in the data analysis.

I. INTRODUCTION

The extended x-ray-absorption fine-structure spectroscopy[1,2] (EXAFS) has been successfully employed for the study of the structural and vibrational behavior of clusters deposited on a noninteracting substrate.[3–5] However, the contraction of the nearest-neighbor (NN) distance and the reduction both of the coordination and of the Debye temperature, obtained for clusters,[4,5] provide average information because of the wide spread of the cluster size distribution on the substrate; in fact, it is not possible to distinguish the different behavior of the surface atoms with respect to the internal ones in clusters with a size-dependent surface-to-volume ratio; or to determine if the clusters agglomerate in geometrical configurations different from that of the bulk crystal.

On the other side, theoretical calculations[6] have deduced for clusters different structures as a function of the size: a 13-atom cluster, e.g., should assume its maximum cohesive energy with a closed-shell icosahedral structure, whereas a 38-atom cluster collapses in a truncated octahedral lattice; even for larger sizes up to 1415 atoms/cluster the truncated octahedral forms seem to be the most favored configurations, whereas far away from the closed truncated octahedral structures, icosahedra are preferred. Unfortunately, to our knowledge no experimental evidence has been reported on the particular structure of a cluster, even though differences, up to 0.14 Å, calculated[6] between the NN distance of the different structures, should be easily resolved. Furthermore, a cluster is a highly asymmetric and polyatomic system, without three-dimensional long-range periodicity. In these cases a strong increase of the static and dynamic disorder is expected mainly because of the higher mobility of the surface atoms, but also for the coexistence of several structural configurations.

In addition, some authors claim that no contraction of the interatomic distance is detected for small metal particles: the experimental work of Montano *et al.*[7] and the theoretical calculations of Hansen *et al.*[8] concur with this conclusion; in contrast Apai *et al.*,[9] D'Agostino, Pinto, and Mobilio,[6] and the present work show a clear contraction of the cluster nearest-neighbor average distance. In the present paper, we studied gold clusters with the aim of distinguishing the structural composition of the clusters contributing to an EXAFS spectrum. To this purpose, the measurements have been performed at $T=28$ K so as to greatly reduce the thermal broadening. Using as a reference a gold layer at the same temperature, we find for clusters significant disorder effects due to the limited spatial dimensions of the cluster and to the asymmetric distribution of the forces in the cluster; additional contributions can be produced by inequivalent sites and by the already mentioned coexistence of different geometrical configurations. Therefore, both standard and cumulant analyses[10,11] have been performed on the exper-

imental spectra. Comparison with theoretical simulations using the method of Rehr and co-workers[12,13] and a specially developed minimization procedure allowed the determination of the geometrical structure in which a cluster condenses.

II. EXPERIMENT

On a thin Mylar substrate we evaporated gold at a very low rate, with a coverage of 5×10^{14} atoms/cm^2, checked by a quartz microbalance. After the gold evaporation, a few monolayers of Mylar were deposited on the evaporated gold particles and this process was repeated many times so as to get a number of Mylar supported clusters piled up: the effective total amount of gold corresponded to a thickness of about 1 μm.

These samples were characterized by means of transmission electron microscopy (TEM). The micrographs confirmed a wide distribution of agglomerates with an apparent spherical shape without any presence of irregular islands; this was expected due to the gold high cohesive energy, and to the negligible interaction with the substrate. The size distribution of the clusters as a function of their diameter is shown in Fig. 1. These samples were analyzed by x-ray-absorption spectroscopy in the range 11.5-13.0 keV around the L_3 absorption edge. Spectra were recorded at $T=28$ K at the Frascati Synchrotron Radiation Laboratory. The x-ray beam was monochromatized by a Si(111) asymmetrical channel-cut crystal and the photons detected by Ar ionization chambers. The resolution of the spectra was about 2 eV. The harmonics content of the monochromatized beam is negligible due to the low critical energy of the bending magnet source used (1.5 keV). In addition, spectra for a gold foil held at the same temperature were collected.

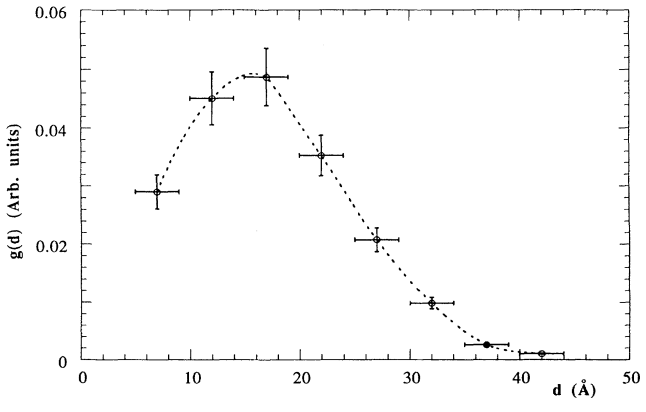

FIG. 1. Number of Au clusters per unit surface of a Mylar substrate, as a function of the diameter. The spectrum was deduced by transmission electron microscopy. The dashed line is a guide to the eye.

III. RESULTS

The x-ray-absorption spectra were analyzed according to a standard procedure:[1,5] the normalized EXAFS oscillations were isolated by subtracting the smooth background fitted by a multiple cubic spline. The EXAFS spectrum $\chi(k)$ is defined as a function of the wave vector k:

$$\chi(k)=[\mu-\mu_0]/\mu_0 d \ ,$$

where $\mu_0 d=J(1-8k^2a^2/3)$ with $a=\hbar/[2mE_0]^{1/2}$, E_0 the threshold energy, and J the jump of the spectrum at the edge.

In fact, the theoretical description of an EXAFS spectrum, including the third and fourth cumulants[10,11] of the radial distribution $\sigma^{(3)},\sigma^{(4)}$, is given by

$$\chi(k)=\sum_j \frac{S_0^2 N_j F_j(k,R_j)}{kR_j^2} \times\exp[-2\sigma_j^2k^2+2\sigma_j^{(4)}k^4/3-2R_j/\lambda(k)] \times\sin[2kR_j+\delta_j(k)-4\sigma_j^{(3)}k^3/3] \ , \quad (1)$$

where S_0^2 is the many-body overlap term, $\lambda(k)$ the electron mean free path; the sum is over the j coordination shell put at a distance R_j from the absorbing atom; $F_j(k,R_j)$ is the atomic backscattering amplitude, δ_j the phase shift of the jth coordination shell, and σ_j^2 the corresponding Debye-Waller (DW) factor.

In Fig. 2 the x-ray EXAFS spectra are shown both for the cluster sample and for the reference Au foil. These curves, weighted by k^3 have been Fourier transformed (Fig. 3). In the Fourier transform (FT) of the gold foil, four coordination shells are clearly visible whereas for clusters only a broad peak due to the first nearest-neighbor coordination sphere is present. This result, as expected, is caused by the short-range order in the clusters and their large thermal disorder. Furthermore, in Fig. 3 it is evident the NN distance contraction and a large broadening typical of atoms vibrating with enhanced amplitude distribution around their equilibri-

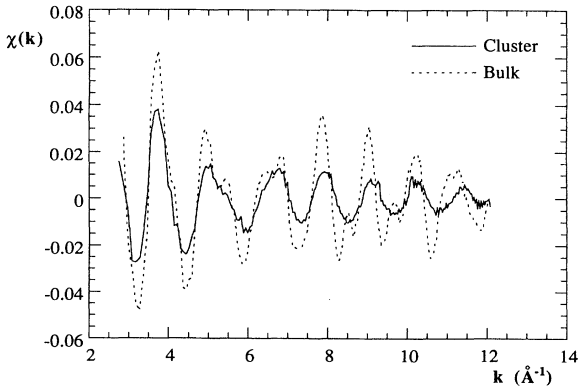

FIG. 2. Measured EXAFS spectra as a function of the wave vector for a gold foil and for the cluster sample.

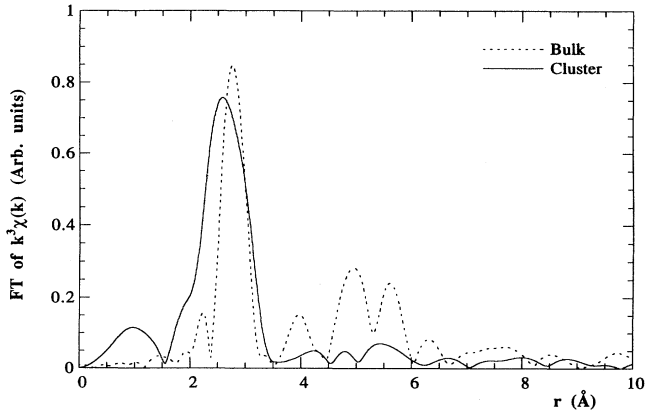

FIG. 3. Fourier transform of the EXAFS spectrum, weighted by k^3, in the real space. The range of the FT of the bulk spectrum was from 2.94 up to 16.1 Å^{-1}; for the cluster spectrum from 2.94 up to 12.2 Å^{-1}, both with a Gaussian window. For the bulk Au foil, the first shell peak and three successive coordination shells are clearly visible; for the cluster sample only the first one is present: the peak corresponds to a lower NN distance from the central atom, with a larger broadening due to the higher mean-square relative displacement.

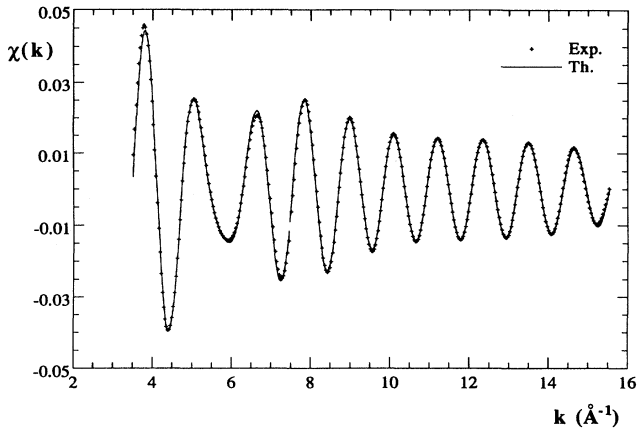

FIG. 4. Bulk Au EXAFS spectrum $\chi(k)$ for the first coordination shell obtained by backtransforming the first shell peak of Fig. 3. The continuous line represents the calculated spectrum using the corresponding parameters of Table I.

um value. In order to get a better understanding of the cluster behavior we used the first shell of the gold foil as a reference: the NN peak was backtransformed in the k space and compared with the theoretical simulation performed for bulk by the method of Rehr and coworkers;[12,13] this last theoretical procedure takes into account curved wave effects, multiple scattering paths, and inelastic losses.[12–14]

In Fig. 4 the bulk gold experimental $\chi(k)$ for the first coordination shell, extracted as mentioned above, is compared with the corresponding theoretical simulation; the excellent agreement between experiment and theory allows us to use the previous data and the related parameters as a reference for the many-body factor S_0, the backscattering amplitude, and the phase shift. In Table I, the first shell parameters of the bulk gold are reported: the values of R and σ^2 are in agreement with those previously published,[3,4] and with those reported in Ref. 15.

In order to improve the statistical accuracy, many spectra have been collected for each experimental configuration, and an accurate statistical analysis was performed with respect to the reference EXAFS spectrum, according to the standard method[14] using the χ^2 expression

$$\chi^2=\frac{N_{pt}}{N(N_{pt}-p)}\sum_i^N \frac{[\chi_{\text{expt}}(k_i)-\chi_{\text{ref}}(k_i)]^2}{s_i^2} ,$$

where N_{pt} are the number of independent data points,[14] p the number of fit parameters, N all data points, and s_i^2 the standard deviation of each data point.

The uncertainties on the parameters of Table I have been calculated by doubling the residual at the minimum: our estimates compare with those of Ref. 15 both for the NN distance and for the DW factor. Furthermore, we point out that the value we used for $S_0^2=1.14\pm0.04$ is larger than 1 for matching the experimental amplitude; as shown in Ref. 12 (Table I), this is often the case when the influence of the electron inelastic contribution λ can be somewhat underestimated: as a matter of fact we opti-

TABLE I. Values of the parameters entering into the EXAFS analysis for bulk and cluster Au. In the standard analysis the cumulants have been constrained to be zero as for the bulk. The many-body parameter S_0^2 has been determined from the spectrum of bulk Au and fixed in the others: its value is larger than 1, to fit correctly the experimental amplitude (see Ref. 12).

	Bulk	Cluster (standard)	Cluster (cumulant)
N	12 (fixed)	8.0±0.4	9.7±0.5
R (Å)	2.865±0.01	2.81±0.01	2.81±0.01
σ^2 (10^{-3} Å^2)	2.6±0.2	5.6±0.3	9.7±0.6
C_3 (10^{-5} Å^3)	0 (fixed)	0 (fixed)	−3±4
C_4 (10^{-4} Å^4)	0 (fixed)	0 (fixed)	1.0±0.1
ΔE_0 (eV)	8.0±0.6	7.1±0.4	7.1±0.4
S_0^2	1.10±0.04	1.10 (fixed)	1.10 (fixed)

mized the value of S_0^2 for the bulk crystal where $N=12$, fixing its value elsewhere.

As clearly indicated in Table I, the values of the third and fourth cumulants were constrained to be zero, since for bulk crystals they are usually negligible.[7] After determining the S_0^2 many-body factor, and the first shell phase and amplitude, by means of the bulk reference spectrum, we analyzed the cluster data with respect to the crystal by the usual comparison[1,5] between the amplitudes A_b and A_c and the total phases ϕ_b and ϕ_c of the bulk and the clusters, respectively; with reference to the first shell only, we write

$$\ln[A_b/A_c]=\ln[N_bR_c^2/N_cR_b^2] - 2\sigma^{(4)}k^4/3-2k^2[\sigma_b^2-\sigma_c^2]\ , \quad (2)$$

$$\phi_b-\phi_c=2k[R_b-R_c]+4\sigma^{(3)}k^3/3\ . \quad (3)$$

The results obtained by fitting the previous expressions as a function of k, with or without constraining the cumulants to be zero, are reported in Table I. We observe that the analysis including the fourth cumulant strongly modifies the coordination number and the Debye-Waller factor, increasing them by about 20% and 70%, respectively. On the contrary, negligible effect is caused by the third cumulant; in fact, no change, within the experimental uncertainty, is found in the absolute value of R, the results of which contracted 0.05 Å with respect to the bulk value. However, as shown in Fig. 5, the comparison of the experimental $\chi(k)$ with the calculated one gives a better agreement if the cumulants are taken into account. This result, although immediately evident in Fig. 5, is confirmed by the χ^2 values ($\chi^2_{\rm cum}=0.17$, $\chi^2_{\rm st}=0.67$). This conclusion was expected because two more free parameters, i.e., the third and fourth cumulants, enter now into the fitting procedure.

However, it is not possible, at the moment, to choose between the standard or the cumulant parameters appearing in Table I, or to decide if the values obtained for the first shell distance, coordination number, and Debye-Waller factor are peculiar to a particular cluster structure or if, on the contrary, they result only as an average between several possible cluster shapes.

Hence an adequate decision requires a comparison with realistic model compounds for size selected clusters; actually, theoretical calculations[6] using a tight-binding potential method have estimated ground-state energy, geometrical configuration, and vibrational properties for gold clusters of different structures and sizes. In Table II cluster data are reported for various closed-shell structures (icosahedral, cubo-octahedral, truncated octahedral) with the number of atoms going from 13 up to 586. It appears evident that the contraction of the nearest-neighbor distance $R=r$ is higher for small agglomerates with low coordination; the average DW factor of the first shell dispersion σ^2 takes into account the different vibrational behavior of surface atoms with respect to internal ones; but, it is strongly influenced by the more compact structure such as the icosahedral, for which the cohesive energy E is higher. Comparing the cluster data of Table II with the experimental values of Table I, no correspon-

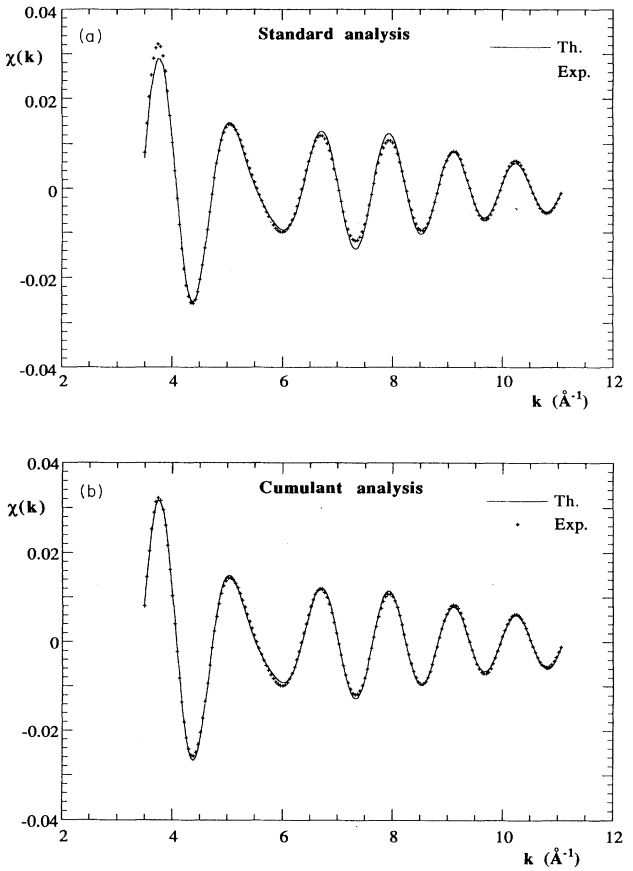

FIG. 5. Comparison of the experimental first shell $\chi(k)$ with the theoretical one calculated using the parameters of Table I: (a) standard analysis, for which the values of the cumulants have been constrained to be zero; (b) cumulant analysis, for which the third cumulant $C_3=4\sigma^{(3)}/3$, and the fourth cumulant $C_4=2\sigma^{(4)}/3$, have been deduced by the best fit of Eqs. (2) and (3), vs k. Note that in case (b) two more free parameters determine an apparent better agreement with the experiment.

TABLE II. List of cluster structures with the corresponding calculated parameters for the size d, the NN distance r, the coordination number N, the DW factor σ^2, and the cohesive energy per atom E (see Ref. 6).

Structures	d (Å)	r (Å)	N	σ^{-2} (10^{-3} Å^2)	E (eV/atom)
13 cubo-oc.	8.28	2.701	5.54	1.98	−3.240
13 icos.	8.18	2.745	6.46	6.09	−3.273
38 trunc.	11.6	2.779	7.58	6.05	−3.432
55 cubo-oc.	13.8	2.784	7.86	4.62	−3.463
55 icos.	13.6	2.811	8.51	8.04	−3.468
147 cubo-oc.	19.5	2.814	8.98	4.62	−3.543
147 icos.	19.1	2.834	9.47	7.87	−3.555
201 trunc.	20.5	2.827	9.43	4.52	−3.586
309 cubo-oc.	25.2	2.830	9.63	4.16	−3.599
309 icos.	25.4	2.846	10.0	7.65	−3.603
561 cubo-oc.	30.8	2.839	10.0	3.83	−3.632
561 icos.	30.1	2.851	10.4	7.01	−3.634
586 trunc.	29.5	2.842	10.2	3.69	−3.645

dence can be found between calculated and experimental parameters. This observation, along with the mass spectral distribution of Fig. 1, can lead to the hypothesis that a mixture of the different situations depicted in Table II constitutes the effective cluster population. This suggestion seems confirmed by comparing (see Fig. 6) the experimental $\chi(k)$ with the EXAFS first shell spectrum simulated for a 38- and 201-atom truncated-octahedron, using the parameters of Table II. Even larger disagreement is found for other structures.

This result is not surprising in view of the mixture of different cluster sizes in the prepared sample. In fact, we remark that the experimental data assume intermediate values between those corresponding to the hypothetical structures: it is then obvious to try a systematic comparison of the experimental curve with a linear combination of the EXAFS contributions coming from all the structural configurations; in other terms we can use a minimization procedure which combines the first shell spectra $\chi_i(k)$ of the ith structure with normalized weights a_i, i.e.,

$$\chi(k)=\sum_i a_i\chi_i(k)$$

for a best fit of the experimental curve. Here, the coefficients a_i should be found by a least-squares method: this corresponds to a decomposition of the experimental curve in components of a given size belonging to a well-defined structure. It is worth pointing out that the structures listed in Table II have statistical weights for each size depending on their thermodynamic free energy, according to Table III. This implies that a cluster can sometimes collapse in two inequivalent structures.

Performing now the minimization procedure as mentioned above, we found that only the structures with 38, 201, and 309 atoms enter into this decomposition with percentages of 85%, 10%, and 5% (see Table IV). The striking conclusion of this result is that the preferred clusterization lattice is truncated octahedral with only 4.2% of icosahedral and 0.8% of cubo-octahedral structure. Using these percentages we get the final combination of cluster structures optimizing the agreement with the experimental $\chi(k)$ as shown in Fig. 7 ($\chi^2_{\min}=0.35$).

We observe that our optimization procedure[16] gives a result in fair agreement with the values obtainable for the cluster parameters R, N, and σ^2, by means of a weighted average of the corresponding theoretical data of Table II; of course, the previous percentages of cluster structures should be modified to take into account the number of atoms per cluster. This gives the following weights: 0.476, 0.296, 0.191, 0.037, respectively, for the number of atoms with structure 38-atom and 201-atom truncated octahedral, 309-atom icosahedral, and 309-atom cubo-octahedral. The average values obtained using these weights and the data of Table II are

$$R=2.808\ \text{Å},\quad N=8.66,\quad \sigma^2=5.83\times10^{-3}\ \text{Å}^2,$$

in qualitative agreement with those given by the minimization procedure.

Furthermore, we note that the presence of a single cluster structure, like the 55-atom icosahedral, to which, e.g., the experimental NN distance is closer, can be excluded since the TEM micrograph (see Fig. 1) confirms a variety of cluster sizes. This is corroborated by the χ^2

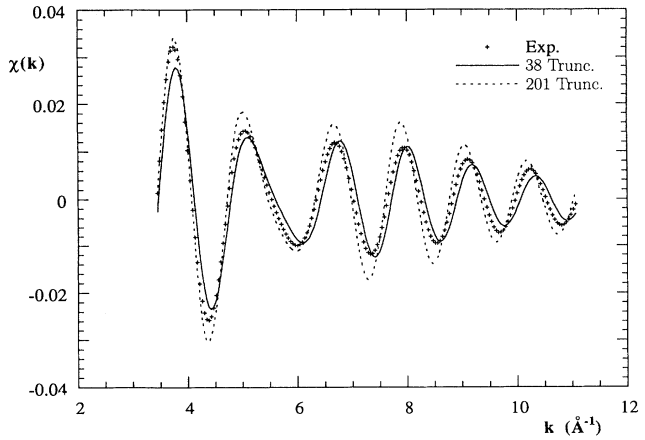

FIG. 6. Comparison of the experimental first shell $\chi(k)$ with the correspondent simulation for two clusters structures with 38 and 201 atoms, respectively. Both structures are truncated octahedral. The parameters are those of Table II.

TABLE III. Thermodynamic statistical factors of the structures listed in Table II, determined as $\exp(-E/kT)$ using the free energy E of the cluster calculated according to Ref. 6.

Size (atoms/cluster)	Cubo-oc.	Icos.	Trunc.
13	0.0	100.0	
38			100.0
55	11.2	88.8	
147	0.7	99.3	
201			100.0
309	16.0	84.0	
561	30.4	69.6	
586			100.0

TABLE IV. Percentages given by the best-fit decomposition of the experimental $\chi(k)$ in terms of size selected structures, as given by Tables II and III.

Size (atoms/cluster)	Percentage (%)
13	0.00±0.01
38	85±10
55	0.00±0.01
147	0.00±0.01
201	10±2
309	5.0±0.4
561	0.00±0.01
586	0.00±0.01

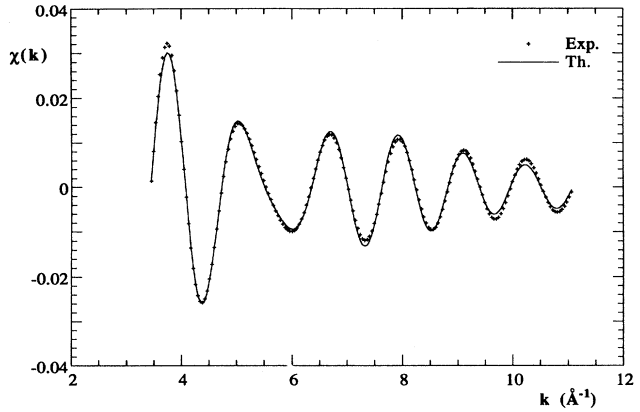

FIG. 7. Comparison of the experimental first shell $\chi(k)$ with the simulation resulting by mixing the percentages shown in Table IV.

values larger by at least a factor of 2 for any single structure.

IV. DISCUSSION

We are now able to discriminate between the approach using the standard analysis against the cumulant fitting of the experimental data, as presented in Table I. Both methods give the same NN distance contraction since the phase fitted in Eq. (3) by an odd function of k is not influenced by the negligible value of the third cumulant $\sigma^{(3)}$. We note also that our value 2.81 ± 0.01 Å determined for the cluster average NN length is in close agreement with the Au-Au distance found for Au_{55} agglomerates in Ref. 15.

On the contrary, the high correlation between the fourth cumulant, the coordination, and the DW factor causes large discrepancies between the values deduced in the two approaches: however, the minimization fitting procedure indicates that the preferred structures are only those contributing at smaller DW and coordination; then, we conclude that the standard analysis gives the most reliable values for the searched parameters. As a consequence, the fourth cumulant is zero or quite negligible, as it should be when the harmonic approximation gives an adequate description of the vibrational properties of the cluster. In Ref. 6 in fact, the anharmonic terms have been ignored so that the mutual consistency of the theoretical calculations with the present data seems fully demonstrated. We point out that our value of σ^2 is at variance with that of Ref. 15 where a hardening of the clusters is found with respect to the bulk. Instead, our data show an amplified mean square relative displacement: let us consider in addition that a larger phonon dispersion is found for gold cluster core levels,[17] and that, in general, for metal surface atoms an enhanced vibrational broadening has been detected[18] with respect to the bulk.

One might suppose a possible asymmetrical distribution of the vibrational equilibrium positions of the cluster atoms, in particular for the shallow part of the cluster; but also this hypothesis can be ruled out as a consequence of the negligible value of the cumulants: these, in fact, being the moments of the radial distribution, measure how much asymmetry there is around equilibrium.

Finally, we want to compare our results with those of Refs. 19 and 20 on Au_{55} clusters stabilized by organic ligands. Here too, as in the present measurements, contraction of the NN distance in the cluster is found with respect to the bulk gold; however, our value (2.81 Å) is larger than that of the Au_{55} cluster: this confirms, as previously demonstrated, that in our case a mixture of different sizes is present. On the contrary, our DW values are significantly lower than those of Refs. 19 and 20: this can be ascribed to the lower temperature of the present experiment and to the presence of ligands in the Au_{55} clusters.

In conclusion, from the EXAFS spectrum of a cluster sample we find several interesting properties: the contraction of the NN distance, the reduction of the average coordination, and the amplification of the mean square relative displacement have been directly deduced by a standard analysis where the third and fourth cumulants are negligible; therefore the clusters behave as systems of atoms bound by harmonic forces without relevant distortions, but agglomerating in particular structures; the truncated octahedral ones seem to participate almost entirely in the composition of the experimental EXAFS spectrum.

ACKNOWLEDGMENTS

The authors would like to thank Professor P. Picozzi and Professor S. Santucci for their hospitality during the preparation of the cluster samples. Thanks are due also to M. Diociaiuti for the electron microscopy measurements.

[1]P. A. Lee, P. H. Citrin, P. Eisenberger, and B. M. Kincaid, Rev. Mod. Phys. **53**, 769 (1981).
[2]E. A. Stern, B. A. Bunker, and S. M. Heald, Phys. Rev. B **21**, 5521 (1980).
[3]A. Balerna, E. Bernieri, P. Picozzi, A. Reale, S. Santucci, E. Burattini, and S. Mobilio, Phys. Rev. B **21**, 5058 (1985).
[4]A. Balerna and S. Mobilio, Phys. Rev. B **34**, 2293 (1986).
[5]G. Faraci, S. La Rosa, A. R. Pennisi, S. Mobilio, and I. Pollini, Phys. Rev. B **45**, 9357 (1992).
[6]G. D'Agostino, A. Pinto, and S. Mobilio, Phys. Rev. B **48**, 14 447 (1993).
[7]P. A. Montano, G. K. Shenoy, E. E. Alp, W. Schulze, and J. Urban, Phys. Rev. Lett. **56**, 2076 (1986).
[8]L. B. Hansen, P. Stoltze, J. K. Norskov, B. S. Clausen, and W.

Niemann, Phys. Rev. Lett. **64**, 3155 (1990).
[9]G. Apai, J. F. Hamilton, J. Stör, and A. Thompson, Phys. Rev. Lett. **43**, 165 (1979).
[10]J. M. Tranquada and R. Ingalls, Phys. Rev. B **28**, 3520 (1983).
[11]D. R. Sandstrom, E. C. Marques, V. A. Biebesheimer, F. W. Lytle, and R. B. Greegor, Phys. Rev. B **32**, 3541 (1985).
[12]J. Mustre de Leon, J. J. Rehr, S. I. Zabinsky, and R. C. Alberts, Phys. Rev. B **44**, 4146 (1991).
[13]J. J. Rehr, R. C. Alberts, and S. I. Zabinsky, Phys. Rev. Lett. **69**, 3397 (1992).
[14]B. Lengeler and P. Eisenberger, Phys. Rev. B **21**, 4507 (1980); F. W. Lytle, D. E. Sayers, and E. A. Stern, Physica B **158**, 701 (1989).
[15]M. A. Markus, M. P. Andrews, J. Zegenhagen, A. S. Bommannavar, and P. Montano, Phys. Rev. B **42**, 3312 (1990).
[16]The fitting procedure is described in the MINUIT program available from the CERN (Centre Europeenne pour la Recherche Nucleaire, Geneva, Switzerland).
[17]E. Costanzo, G. Faraci, A. R. Pennisi, S. Ravesi, A. Terrasi, and G. Margaritondo, Solid State Commun. **81**, 155 (1992); G. Faraci, E. Costanzo, A. R. Pennisi, Y. Hwu, and G. Margaritondo, Z. Phys. D. **23**, 263 (1992).
[18]D. M. Riffe, G. K. Wertheim, and P. H. Citrin, Phys. Rev. Lett. **67**, 116 (1991).
[19]M. C. Fairbanks, R. E. Benfield, R. J. Newport, and G. Schmid, Solid State Commun. **73**, 431 (1990).
[20]P. D. Cluskey, R. J. Newport, R. E. Benfield, S. J. Gurman, and G. Schmid, Z. Phys. D **26**, S8 (1993).